CrossMark

Temperature sensitivity of Fe-substituted SnO₂-based ceramics as negative temperature coefficient thermistors

Jia Zhang[1] · Hong Zhang[1,3] · Bao Yang[1] · Yu Zhang[1] · Zhicheng Li[1,2]

Abstract Sb-doped SnO₂ (ATO) and Fe-substituted ATO [$Sn_{0.95-y}Sb_{0.05}Fe_yO_2\,(y \leq 0.10)$] ceramics were prepared by using a wet chemical process followed by high-temperature solid reaction, and the related electrical conductivities were investigated. The analysis of X-ray diffraction indicates that all the prepared ceramics have a tetragonal crystal structure as that of rutile-type SnO₂. The room-temperature resistivity ρ_{25} of the Fe-substituted ATO increases with the Fe-content rising, and the Fe-substituted ATO ceramics show a typical characteristic of negative temperature coefficient (NTC) of resistivity. Compared with the ATO ceramics, the substitution of Fe can obviously adjust the materials constant $B_{25/85}$ as NTC thermistors. Fe-substituted ATO ceramics show high cyclic stability between room temperature and 250 °C. The investigations of electrochemistry impedance spectra reveal that the grain boundary effect is dominant in the NTC feature. Both the band conduction and electron-hopping models are proposed for the conduction mechanisms in the Fe-substituted ATO ceramics.

1 Introduction

Thermistors with a characteristic of negative temperature coefficient (NTC) of resistivity are extensively applicable in various fields such as circuit compensation, aerospace, solar cells, automotive temperature measurement and control applications, owing to its high temperature sensitivity [1–3]. Traditional NTC ceramic thermistors are usually comprised of transition-metal oxides with a spinel structure, e.g., Mn–Ni–O, Ni–Cu–Mn–O and Mn–Co–Ni–O systems, etc. [4–6]. However, for the structural relaxation and property degradation taken place in those compounds, the NTC application is constrained with the low temperature region (below 200 °C) [7, 8]. Numerous studies have tried to improve the electrical properties and ageing resistance of the spinel-type thermistors by cation doping and microstructure modification [9, 10], etc. Meanwhile, new types of NTC thermistors have also been constructed recently [11–13].

Tin dioxide (SnO₂), a semiconductor with a band gap of about 3.5 eV, shows wide applications for various devices such as gas-sensors, flat panel display and electrodes for lithium-ion batteries [14–16]. Extensive investigations for the varistors of SnO₂ have been conducted for that the electrical properties can be enhanced significantly by doping with dopants such as Sb₂O₃, Bi₂O₃, Cr₂O₃ and In₂O₃, etc. [17, 18]. Saadedin et al. reported that the antimony-doped tin dioxide (ATO) exhibited good electrical properties with a high conductivity [19], and Zn/Sb co-doped SnO₂ exhibits a high electrical conductivity. For the actual applications of NTC thermistors, a suitable ρ_{25} and high $B_{25/85}$ value are always required. Like most of the semiconductors, although ATO ceramics may display the NTC characteristic, they suffer from a typical shortcoming such as a high material constant $B_{25/85}$ accompanied by a

✉ Zhicheng Li
zhchli@csu.edu.cn

1 School of Materials Science and Engineering, Central South University, Changsha 410083, China

2 State Key Laboratory of Powder Metallurgy, Central South University, Changsha 410083, China

3 Institute for Materials Microstructure, Central South University, Changsha 410083, China

high value of room-temperature resistivity ρ_{25} and/or a low ρ_{25} associated with a low $B_{25/85}$, which is far away from the application demand of the NTC thermistors. In order to obtain the desired performance of the ATO ceramics for NTC applications, certain attention has been paid to adding various cations into the ATO. Ouyang et al. reported that the ρ_{25} and $B_{25/85}$ is feasible to be adjusted in $Sn_{0.95}Sb_{0.05}O_2$-$BaTi_{0.8}Fe_{0.2}O_{3-\delta}$ NTC composite ceramics [20], which indicates the great possibility of the materials with adequate performance by controlling addition of $BaTi_{0.8}Fe_{0.2}O_{3-\delta}$. Recent reports showed that it is interesting to obtain the NTC thermistor based on single oxide such as CuO or SnO_2 for that its room-temperature resistivity and NTC materials constant can be easily adjusted with minor amount of substitutions, and the NTC thermistors showed high property stability [21–23].

In present work, to develop a new system of NTC thermistors, Fe-substituted $Sn_{0.95}Sb_{0.05}O_2$ oxides, $Sn_{0.95-x}Sb_{0.05}Fe_yO_2$, were prepared and the electrical properties were investigated by using the analysis of complex impedance and electric modulus spectra.

2 Experimental

$Sn_{1-x}Sb_xO_2$ (ATO, $x = 0, 0.01, 0.02, 0.03, 0.05$ and 0.07) ceramics were prepared by the wet chemical synthesis followed by high-temperature solid reaction method. Initially, appropriate amount of high-purity Sn powder and antimony oxide (Sb_2O_3) powder were weighed according to the formula $Sn_{1-x}Sb_xO_2$ and were dissolved respectively into concentrated nitric acid solution. Then the above dissolution were mixed together, the pH value was adjusted to be about 7 by adding ammonium hydroxide. The mixture was heated under continuous stirring till complete water evaporation. Subsequently, the precursors were calcined at 830 °C for 6 h in air to obtain $Sn_{1-x}Sb_xO_2$ powders. Finally, each as-calcined powders, mixed utterly with 2 mol% $Cu(OH)_2$ as sintering aid, were pressed into the pellets with 12 mm in diameter and about 3 mm in thickness and were subjected to sintering at 1350 °C for 60 min in air.

In order to improve the NTC feature of the ATO ceramics, Fe-substituted $Sn_{0.95}Sb_{0.05}O_2$ ceramics, $Sn_{0.95-y}Sb_{0.05}Fe_yO_2$ (denoted as FATO, $y = 0–0.10$), with ferric citrate as the source of iron, were investigated in the present work. The as-calcined ATO powder, appropriate amount of ferric citrate and 2 mol% of $Cu(OH)_2$ were mixed thoroughly in an agate mortar. The mixed powders were pressed into the pellets with 12 mm in diameter and about 3 mm in thickness. The pellets were subjected to sintering at 1350 °C for 60 min in air. Both opposite surfaces of the as-sintered ceramics were polished and then painted with silver slurry followed by heating at 600 °C in air for making electrodes.

The temperature dependent resistance of each ceramic was measured by using a resistance–temperature measurement system (ZWX-C, China) in the temperature range from room temperature to 250 °C. The X-ray Diffraction (XRD) measurement was carried out by using an X-ray diffractometer (Rigaku D/max 2500, Japan) with Cu K_α radiation at room temperature. Electrical impedance spectra (EIS) of the tested samples were obtained by using an electrochemical measurement system (Gamry Reference 600, USA) in the frequency ranging from 1 MHz to 1 Hz, at the temperature ranging from room temperature to 250 °C. The microstructures of samples were characterized by scanning electron microscopy (SEM, FEI Quanta 200).

3 Results and discussion

3.1 Phase and microstructure

The XRD patterns of the as-sintered FATO ($y = 0.015$, 0.05) ceramics are presented in Fig. 1. All diffraction peaks can be indexed to be the SnO_2 crystal phase with tetragonal rutile structure with a space group of $P4_2/mnm$ (136), according to the powder diffraction file (PDF) number of 41–1445. The absence of any other phases is probably ascribed to the various existing forms of Fe and Cu ions in the ceramics: formation of solid solution, segregation on the surface of grain, together with formation of an amorphous phase. It was reported that the segregation of Fe in the grain boundary of SnO_2 is invisible unless the Fe doped content beyond 20 mol%, which provided a significant support of formation of solid solution of majority of Fe in FATO ceramics [17]. By using Jade 5.0 + pdf2003 program, the lattice parameters are refined to be $a = b = 0.4734$ nm, $c = 0.3185$ nm for the FATO with 1.5 mol% Fe, and $a = b = 0.4732$ nm, $c = 0.3180$ nm for the FATO with Fe
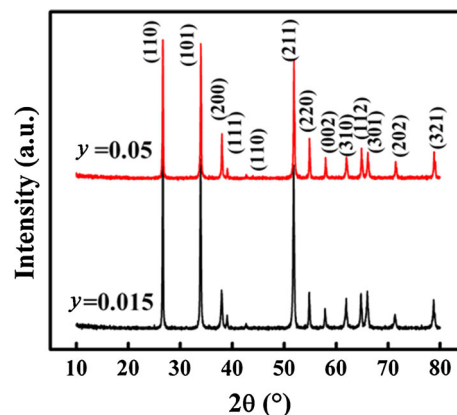
Fig. 1 XRD patterns of the as-sintered $Sn_{0.95-y}Sb_{0.05}Fe_yO_2$ ceramics ($y = 0.015$ and 0.05)

content of 5 mol%. Their lattice parameters are slightly smaller than those of the pure SnO_2 ($a = b = 0.4738$ nm, $c = 0.3187$ nm). These could be ascribed to the radii different between the ones of Fe^{3+} (0.065 nm), Fe^{2+} (0.078 nm), Sb^{5+} (0.061 nm), Sb^{3+} (0.076 nm), Cu^{2+} (0.073 nm) and the one of Sn^{4+} (0.069 nm) [24].

Figure 2a, b show the SEM observations of fracture surface of the as-sintered $Sn_{0.95}Sb_{0.05}O_2$ and $Sn_{0.935}Sb_{0.05}Fe_{0.015}O_2$ ceramics, respectively. Both of the ceramics have the similar microstructures. Unequal grains with the sizes of 2–10 μm can be observed obviously. The grains connect closely to each other. Some small pores locating inside the grains, which might resulted from the quick temperature increasing during the sintering for that gas could not volatilize sufficiently from the pellet.

3.2 Temperature dependence of resistivity

The resistivity of each measured resistance was calculated according to the sample size. Plots of the logarithmic resistivity (lnρ) versus the reciprocal absolute temperature of the ATO ceramics with various contents of Sb are shown in Fig. 3a. It is clearly observed that all the lnρ-1/T plots exhibit the linear relationship. The undoped SnO_2 ceramic, with a large ρ_{25} of 1.39×10^5 Ω cm and materials

Fig. 2 SEM images of fracture surface of the as-sintered ceramics, **a** $Sn_{0.95}Sb_{0.05}O_2$, **b** $Sn_{0.935}Sb_{0.05}Fe_{0.015}O_2$

constant B of 4998 K, displays a typical NTC characteristic. However, the Sb-doped SnO_2 ceramics, regardless of Sb doping content, have the ρ_{25} lower than 50 Ω cm and do not have obvious temperature sensitivity of resistivity. These indicate that the conductivities of SnO_2 are evidently decorated by the Sb-doping, but the Sb-doped SnO_2 has no available NTC effect.

Figure 3b illustrates the temperature dependence of resistivity of the Fe-doped $Sn_{0.95}Sb_{0.05}O_2$ ceramics. The room-temperature resistivity of the FATO ceramics increases with the increasing of Fe content. For each sample, the resistivities monotonically decrease with the temperature increasing, indicating a typical NTC behavior of the FATO ceramics. Comparing Fig. 3a with Fig. 3b, it is found that the substitution of Fe makes it easy to adjust the ρ_{25} and $B_{25/85}$ of the ATO ceramics, which provides a great potential for the real applications as NTC themistors. Moreover, it is efficient to acquire the NTC thermistors with desired electrical properties by co-doping of Fe and Sb. The plots of temperature-dependent resistivity of FATO ceramics with various Fe contents almost comply with the Arrhenius relationship as shown in Eq. (1).

$$\rho = \rho_0 \exp\left(\frac{E_a}{kT}\right) \tag{1}$$

where, ρ is the resistivity at temperature T, ρ_0 is the pre-exponential factor related to the material characteristic, E_a is the activation energy of conduction, k is the Boltzmann constant and T is the absolute temperature. Clearly, subtle difference among the slopes of the plots can be seen in the different temperature regions, the details are shown Table 1. This phenomenon should be due to the different conduction mechanisms existing in the different temperature regions, and will be discussed in detail in next section.

The NTC materials constant $B_{25/85}$ of the FATO ceramic can be calculated according to Eq. (2).

$$B_{25/85} = \frac{\ln \rho_{25} - \ln \rho_{85}}{(1/T_{25}) - (1/T_{85})} \tag{2}$$

where, ρ_{25} and ρ_{85} stand for the resistivity at 25 and 85 °C, respectively. The $B_{25/85}$ of FATO ceramics with the Fe contents varying from 0 to 5 mol% are demonstrated in Fig. 3c. One can see that ρ_{25} and $B_{25/85}$ can be effectively adjusted by changing the Fe content in the FATO ceramics. It is well received that the introducing of Fe to the SnO_2 lattice might cause the lattice distortion for the different radii and valences, resulting in the rise of resistivity. Meanwhile, although the XRD result gives an evidence of majority of Fe existing in the state of solid solution, there should still be minimal amount of Fe segregating at the grain boundary to hinder the mobility of charge carrier [17], leading to the increase of resistivity. On the other hand, the presence of numerous remnant charge carriers,
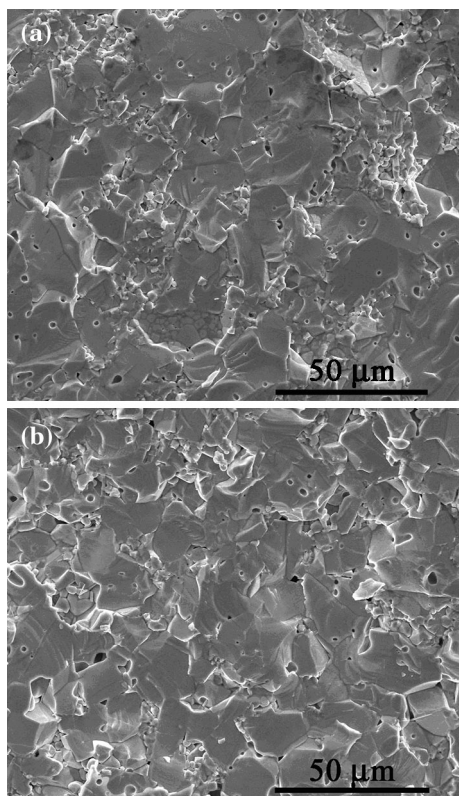
Fig. 3 Electrical properties of SnO$_2$-based NTC thermistors, **a** temperature dependence of resistivity of Sn$_{1-x}$Sb$_x$O$_2$ ceramics, **b** temperature dependence of resistivity of Sn$_{0.95-y}$Sb$_{0.05}$Fe$_y$O$_2$ ceramics, **c** influence of Fe-content, y, on the room-temperature resistivity (lnρ_{25}) and NTC materials constant ($B_{25/85}$), **d** repeatability of the temperature dependence of resistivity of a Sn$_{0.935}$Sb$_{0.05}$Fe$_{0.015}$O$_2$ ceramic
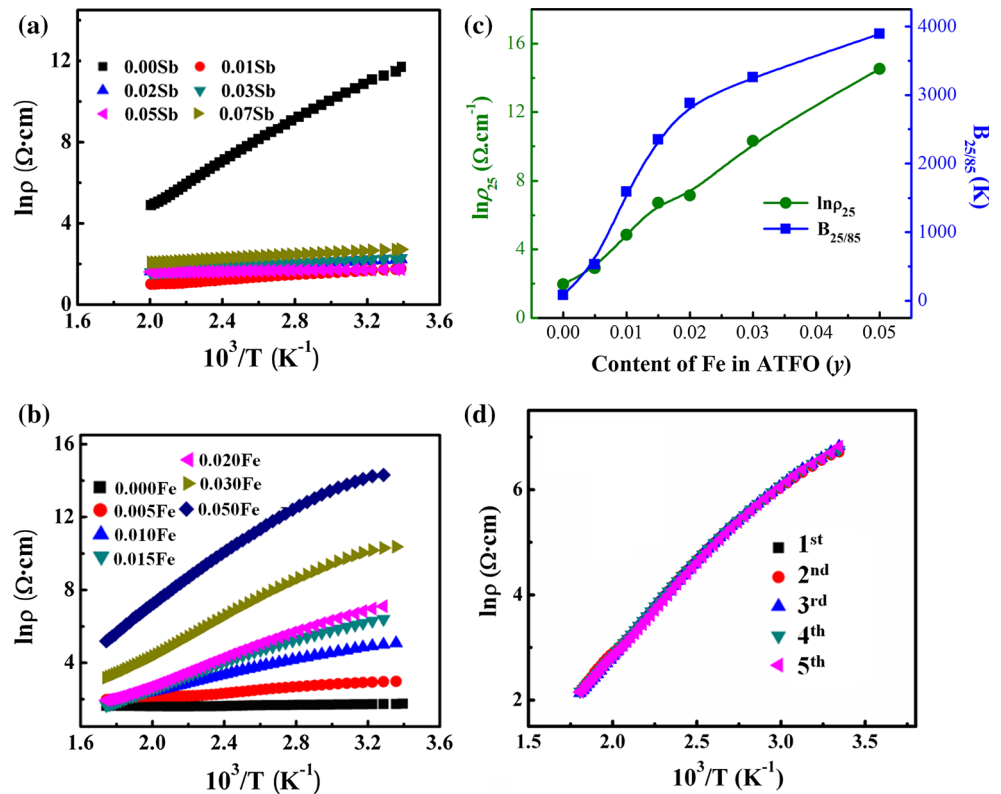
Table 1 Room temperature resistivity ρ_{25} and activation energy E_a of Sn$_{0.95-y}$Sb$_{0.05}$Fe$_y$O$_2$ ceramics in different temperature ranges

y	ρ_{25} (Ω cm)	<120 °C E_a (eV)	120–150 °C E_a (eV)	>150 °C E_a (eV)
0.01	1.60×10^2	0.15	0.19	0.19
0.015	6.04×10^2	0.22	0.29	0.32
0.02	1.22×10^3	0.26	0.33	0.33
0.03	3.19×10^4	0.35	0.46	0.46
0.05	1.65×10^6	0.39	0.55	0.62

including the released electrons and electron holes created in the complementary substitution of Fe, Cu and Sb with Sn, may also result in the conductivity decline.

It is well known that stability is considered as a necessary premise for the applications. Figure 3d shows the temperature dependence of resistivity of a Sn$_{0.935}$Sb$_{0.05}$-Fe$_{0.015}$O$_2$ ceramic measured repeatedly for 5 times. All the plots exhibit a centralized data distribution in the temperature range, revealing a good reproducibility property and high stability.

3.3 AC electrical property

There are generally two main possible mechanisms, hopping model and band conduction one, contributing to the conduction of a NTC ceramic. And the conductivity increases exponentially with temperature rising. The small-polaron hopping model is a typical conduction mechanism for the traditional NTC ceramics composed of transition-metal compounds, especially for spinel-style ceramics [25, 26]. In hopping model, the conductivity is correlated with temperature and frequency. In band conduction model, the conductivity is independent of frequency and is influenced by temperature. Alternative current (AC) impedance spectrum measurement is usually regarded as one of the powerful tools to investigate the electrical property of a NTC thermistor. The impedance data $Z(\omega)$ is usually plotted in the Cole–Cole plane according to Eq. (3).

$$Z(\omega) = Z'(\omega) + jZ''(\omega) \tag{3}$$

where, $\sqrt{j} = -1$, ω is the angular frequency ($\omega = 2\pi f$), Z' and Z'' are the real and imaginary parts of the complex impedance, respectively. And the complex admittance $\sigma(\omega)$ was obtained by complex impedance according to $\sigma(\omega) = 1/Z(\omega)$. The frequency-dependent ac conductivity $\sigma'(\omega)$, the response of the real part of $\sigma(\omega)$, can be calculated by employing the formula of $\sigma'(\omega) = Z'(\omega)/|Z|^2$.

The logarithmic $\sigma'(\omega)$ as a function of logarithmic frequency (logω) of a Sn$_{0.935}$Sb$_{0.05}$Fe$_{0.015}$O$_2$ ceramic at different temperatures is shown in Fig. 4a. The AC conductivity $\sigma'(\omega)$ is independent of frequency in low frequency region, but increases with the rise of frequency in high frequency region. Meanwhile, as the temperature

increased from 30 to 150 °C, the conductivity increased correspondingly. The frequency value corresponding to the turnover point of $\sigma'(\omega)$ plots shifts to higher frequency with the temperature elevated. It indicates that the band conduction, resulted from the doping effect by Sb^{5+}, Sb^{3+} and even Fe-ions and Cu-ions, plays a significant role in the conductivity behavior of $Sn_{0.935}Sb_{0.05}Fe_{0.015}O_2$ ceramic in lower frequency region, while the conduction behavior is mainly governed by the hopping conduction in high frequency region.

In the FATO ceramics, the localized charge carriers are usually considered to be the Sb-ions and Fe-ions with variable valences. The hopping processes are closely associated with the substitution of Fe with Sn accompanying with the electron escaping and the replacement of Sb with Sn producing surplus electron or electron hole. The hopping processes of the localized charge carriers of Fe^{3+} can be described as $Fe^{3+}+Fe^{2+} \leftrightarrow Fe^{2+}+Fe^{3+}$. For the Sb-ion, as hypothesized by Nobre et al. [27], the existence of a transition valence state Sb^{4+} provides a hopping link between Sb^{3+} and Sb^{5+}, such as $Sb^{3+} + Sb^{5+} \leftrightarrow Sb^{4+} \leftrightarrow Sb^{5+} + Sb^{3+}$.

To further explore the conduction mechanisms at different temperature ranges, much attention has been paid to the study of relationship between $\log[\sigma'(\omega)–\sigma'(0)]$ and $\log\omega$. As proposed by Jonscher [28], the frequency dependent conductivity via the hopping of charge carrier can be expressed by Eq. (4).
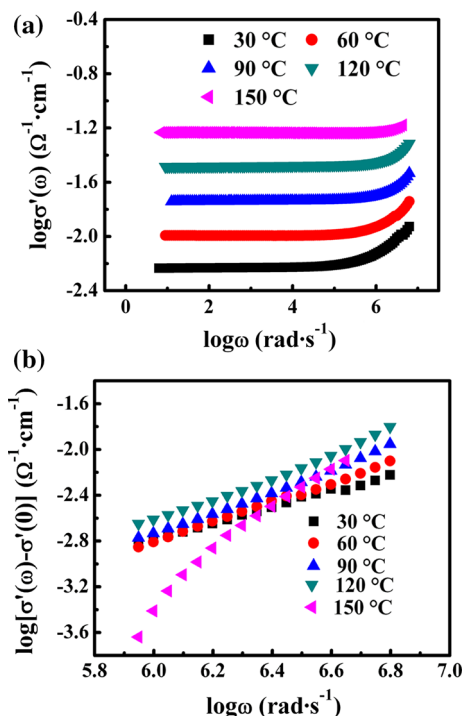

Fig. 4 Angular frequency ω dependence of complex admittance $\sigma'(\omega)$ of a $Sn_{0.935}Sb_{0.05}Fe_{0.015}O_2$ ceramic at different temperatures, **a** $\log\sigma'(\omega)$–$\log\omega$ plots, **b** $\log[\sigma'(\omega)–\sigma'(0)]$–$\log\omega$ plots

$$\sigma'(\omega) = \sigma'(0) + A\omega^n \qquad (4)$$

where, $\sigma'(\omega)$ is the frequency dependent conductivity, $\sigma'(0)$ is the direct current (DC) conductivity which can be extracted from the value of $\sigma'(\omega)$ when ω tend toward zero, A is a thermally activation constant depending upon temperature, n represents the power exponent. When the value of n is less than 1, electrical behavior is governed by hopping conduction [29]. Figure 4b shows the relationship between $\log[\sigma'(\omega)–\sigma'(0)]$ and $\log\omega$ of $Sn_{0.935}Sb_{0.05}Fe_{0.015}O_2$ at various temperatures. Due to the limited resolution of the measurement apparatus, the complex impedance from the grain effect could not be identified at the temperatures higher than 150 °C. It is easy to attain the value of A and n by reading the intercept and slope of the fitted plot using the suitable fitting program. The n values are 0.703, 0.856, 0.951, 0.985 and 1.850 at temperatures of 30, 60, 90, 120 and 150 °C, respectively. In lower temperature region ($\leq$120 °C), the value of n is less than 1, confirming the dominant contribution of hopping conduction in FATO ceramics. The value of n is more than 1 at temperature higher than 120 °C, revealing that electrical properties should result from another conduction behavior besides the hopping conduction.

3.4 Impedance and electric modulus analysis

It is well received that the Nyquist plots of a NTC ceramic are normally composed of two arcs. The one corresponds to the bulk effect in the higher frequency region, while another one is the response of the grain boundary effect in the lower frequency region [30]. Figures 5a, b show the Nyquist plots of a $Sn_{0.935}Sb_{0.05}Fe_{0.015}O_2$ ceramic at 30, 60, 90, 120 and 150 °C, respectively. One can see that each plot is characterized by part of single arc, which can be ascribed to negligible contribution of either grain effect or grain boundary effect. To identify the contribution origin, the plots were fitted by an equivalent circuit of R-RCQ model as shown in the inset in Fig. 5b. Where, R_0 stands for the independent of frequency such as the resistance from the leading wire and contact resistance, R_1, C_1 and CPE_1 represent the resistance, capacitance and constant phase element of the ceramic, respectively.

In Fig. 5a, b, the curve lines are the fitted results and the points are the response of experimental data. The fitted results are in good agreement with the experimental data. The fitted capacitance values (C_1) are 2.44×10^{-9}, 2.82×10^{-9}, 4.85×10^{-9} and 1.293×10^{-8} F at 30, 60, 90 and 120 °C, respectively. As reported by Irvine et al. [31], the capacitance of grain effect is of about 10^{-12} F while the one of grain boundary effect is in the level of 10^{-11} to 10^{-8} F. These indicate that the impedance spectra shown in Fig. 5 should result from the grain boundary
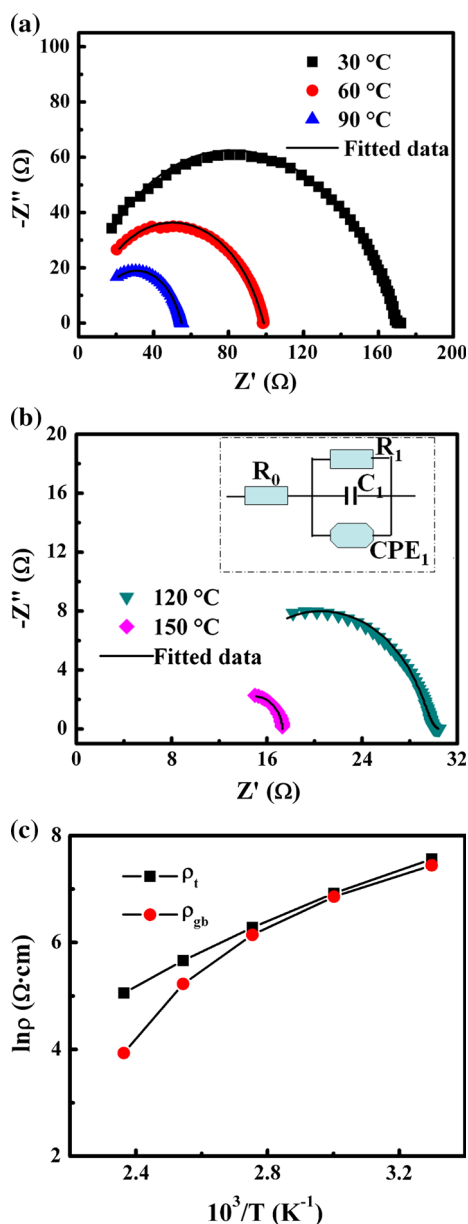
Fig. 5 Electrical properties of a $Sn_{0.935}Sb_{0.05}Fe_{0.015}O_2$ ceramic at different temperatures, **a** Nyquist plots at 30, 60 and 90 °C, **b** Nyquist plots at 120 and 150 °C, and an *inset* equivalent circuit for data fitting, **c** logarithmic resistivity as a function of reciprocal temperature from the grain boundary effect (ρ_{gb}) and the total sample (ρ_t)

contribution of the grain boundary effect to electrical behavior. The significant role of grain boundary effect should be partly ascribed to be the segregation of a small amount of Fe-ions or impurities at the grain boundary region. Besides, the lattice defects caused by the inconsistent substitution at the grain boundary, such as the replace of Sn^{4+} with Fe^{3+} and/or Cu^{2+} in FATO ceramics, should be also responsible for the conduction behavior.

Figure 6a shows the variation of imaginary part (Z'') as a function of logarithmic frequency at various temperatures, and the inset is the magnified drawing of selected part. For each plot, the value of Z'' displays the feature of frequency independence in the lower frequency region, indicating that the electrode polarization is insignificant. As the temperature increases, the magnitude of the relaxation peak decreases monotonically. The relationship between the height of relaxation peak Z'' and the materials resistance (R) can be described as Eq. (5).

$$Z'' = R\left[\frac{\omega\tau}{1 + (\omega\tau)^2}\right] \tag{5}$$

where R represents resistance, ω represents the angular frequency and τ is relaxation time. The relaxation behavior is dependent of the temperature, indicting that the electrical relaxation is a thermally activating process. The relaxation

effect, and the resistance from grain effect is too small to be detected [18]. In addition, the semicircle center of each arc locates below the abscissa axis, indicating the existence of a non-Debye type relaxation behavior.
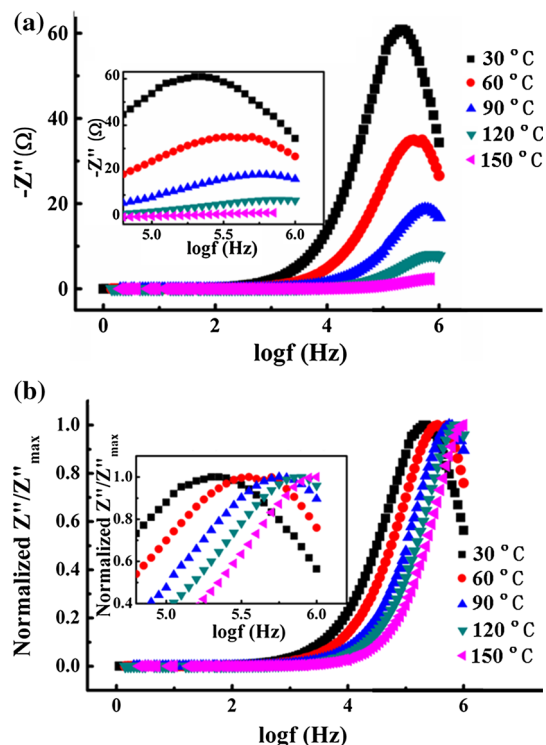
The logarithmic resistivities of the grain boundary effect (ρ_{gb}) and the total effect (ρ_t), obtained from the fitted results, as a function of reciprocal temperature are shown in Fig. 5c. One can see that both ρ_{gb} and ρ_t exhibit the NTC characteristic. Furthermore, ρ_{gb} is basically close to ρ_t in the lower temperature region, suggesting the dominant

Fig. 6 Plots of frequency dependence of imaginary impedance (Z'') of $Sn_{0.935}Sb_{0.05}Fe_{0.015}O_2$ ceramic at various temperatures, **a** plots of $Z''-\log f$, **b** normalized value plots of $Z''/Z''_{max}-\log f$

species is possibly considered to be immobile hole/electron at low temperature and defect/vacancy at high temperature [12]. Figure 6b shows the logarithmic frequency dependence of normalized imaginary part of impedance (Z''/Z''_{max}) and the inset is the located magnified drawing. The peak frequency, namely the corresponding frequency of the maximum of each plot, shifts towards the higher frequency region. This indicates that the relaxation time decreases with the increase of temperature, accompanying the increase of the conductivity.

Both the normalized imaginary impedance (Z''/Z''_{max}) and modulus (M''/M''_{max}) as a function of logarithmic frequency at different temperatures are shown in Fig. 7. The inset plots in Fig. 7b are the magnified drawing of selected part. In the temperature below 120 °C, the obvious mismatch between Z''/Z''_{max} and M''/M''_{max} peaks not only indicates that localized conduction and/or the hopping conduction exist in the ceramics, but also reveals that hopping conduction plays a more significant role. With the temperature rising up to 120 °C, the Z''/Z''_{max} peak overlaps partly with the M''/M''_{max} peak. When the temperature increases up to 150 °C, the two kinds of peaks almost match each other, confirming the presence of band conduction and mirroring that conduction behavior is governed by the long-range conduction.
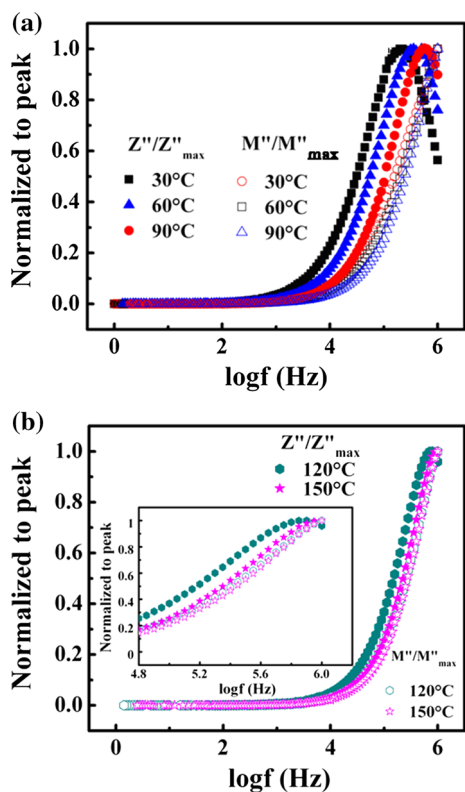
Fig. 7 Plots of frequency dependent normalized imaginary impedance (Z''/Z''_{max}) and normalized electric modulus (M''/M''_{max}) of $Sn_{0.935}Sb_{0.05}Fe_{0.015}O_2$ ceramic, **a** at 30, 60 and 90 °C, **b** 120 and 150 °C

Based on the discussion above, there are two kinds of conduction mechanisms of hopping conduction and band conduction for the electrical property of the FATO ceramics. The band conduction, usually occurring inside the grains, is supposed to the transport process of charge carriers such as electrons and/or electron holes, and is considered to be a long-range transport process. The dopants (donor of Sb^{5+}, and possible acceptors such as Fe^{2+}, Fe^{3+}, Sb^{3+} and Cu^{2+}, etc.) in SnO_2 cause the occurrence of charge carriers, electrons on the donor level and/or electron hole on the acceptor level. All of them play a significant role in enhancing the conductivity of the ceramics. For the small enough resistivity from the grain effect, the band conduction is not the main contributor for the NTC feature in FATO ceramics, although the grain effect resistivity also increases with temperature rising. The hopping conduction, based on the activated electron hopping between ionic pairs, can be expressed as $Fe^{3+} + Fe^{2+} \leftrightarrow Fe^{2+} + Fe^{3+}$ and $Sb^{3+} + Sb^{5+} \leftrightarrow 2Sb^{4+} \leftrightarrow Sb^{5+} + Sb^{3+}$. The hopping conduction may take place inside the grains and at the grain boundaries. The activation effect is enhanced when the temperature increases.

4 Conclusions

$Sn_{1-x}Sb_xO_2$ (ATO, $x = 0$, 0.01, 0.02, 0.03, 0.05 and 0.07) and Fe-substituted $Sn_{0.95}Sb_{0.05}O_2$ (FATO) ceramics were synthesized by the wet chemistry process followed by the high-temperature solid reaction method. All the ceramics have the tetragonal rutile-type SnO_2 phase. Sb-doping in SnO_2 can obviously enhance the conductivity, but the ATO ceramics do not have obvious temperature sensitivity of resistivity. The substitution of Fe can effectively adjust both the room temperature resistivity and materials constant of ATO as NTC thermistors. The FATO thermistors have high cyclic stability and should be useful for the development of high performance NTC thermistor devices. The conduction of the FATO thermistors results from both grain effect and grain-boundary effect, and the grain boundary effect makes the dominant contribution to the NTC effect. Two possible conduction mechanisms of band conduction and hopping conduction are proposed in the FATO thermistors.

References

1. A. Feteira, J. Am. Ceramic. Soc. **92**, 967–983 (2009)

2. J.G. Fagan, V.R.W. Amarakoon, Am. Ceram. Soc. Bull. **72**, 70–79 (1993)
3. G. Lavenuta, Sensors. **14**, 46–55 (1997)
4. M. Suzuki, J. Phys. Chem. Solids **41**, 1253–1260 (1980)
5. R.N. Jadhav, S.N. Mathad, V. Puri, Ceram. Int. **38**, 5181–5188 (2012)
6. F. Fard, S. Golestani, K.J.D. Azimi, J. Mackenzie, Mater. Sci. **22**, 2847–2851 (1987)
7. X.Q. Li, J. Mater. Sci. **19**, 271–274 (2008)
8. A. Feltz, W. Polzl, J. Eur. Ceram. Soc. **20**, 2353–2366 (2000)
9. D.L. Fang, C.S. Chen, A.J.A. Winnubst, J. Alloy. Compd. **454**, 286–291 (2008)
10. D.A. Kukuruznyak, J.D. Moyer, F.S. Ohuchi, J. Am. Ceram. Soc. **89**, 189–192 (2006)
11. M.A.L. Nobre, S. Lanfredi, Appl. Phys. Lett. **82**, 2284–2286 (2003)
12. S.K. Barik, R.N.P. Choudhary, P.K. Mahapatra, J. Mater. Sci. Mater. Electron. **19**, 607–614 (2008)
13. W.T. Chen, F. Sher, N.D. Mathur, C.M. Kavanagh, F.D. Morrison, J.P. Attfield, Chem. Mater. **24**, 199–208 (2011)
14. J. Kaur, J. Shah, R.K. Kotnala, K.C. Verma, Ceram. Int. **38**, 5563–5570 (2012)
15. S. Yu, W. Zhang, L. Li, D. Xu, H. Dong, Y. Jin, Appl. Surf. Sci. **286**, 417–420 (2013)
16. M.C. Esteves, D. Gouvêa, P.T.A. Sumodjo, Appl. Surf. Sci. **229**, 24–29 (2004)
17. A.C. Antunes, S.R.M. Antunes, A.J. Zara, S.A. Pianaro, E. Longo, J.A. Varela, J. Mater. Sci. **37**, 2407–2411 (2002)
18. P.R. Bueno, J.A. Varela, E. Longo, J. Eur. Ceram. Soc. **28**, 505–529 (2008)
19. I. Saadeddin, H.S. Hilal, B. Pecquenard, J. Marcus, A. Mansouri, C. Labrugere, M.A. Subramanian, G. Campet, Solid State Sci. **8**, 7–13 (2006)
20. P. Ouyang, H. Zhang, D. Xue, Z. Li, J. Mater. Sci. Mater. Electron. **24**, 3932–3939 (2013)
21. Y. Zhang, Y. Wu, H. Zhang, W. Chen, G. Wang, Z. Li, J. Mater. Sci. Mater. Electron. **25**, 5552–5559 (2014)
22. P. Ouyang, H. Zhang, Y. Zhang, J. Wang, Z. Li, J. Mater. Sci. Mater. Electron. **26**, 6163–6169 (2015)
23. B. Yang, H. Zhang, J. Zhang, X. Zhang, Z. Li, J. Mater. Sci. Mater. Electron. DOI: 10.1007/s10854-015-3701-0
24. R.D. Shannon, Acta Crystallogr. A **32**, 751–767 (1976)
25. R. Schmidt, A.W. Brinkman, J. Appl. Phys. **103**, 113710 (2008)
26. S. Brahma, R.N.P. Choudhary, A.K. Thakur, Phys. B Cond. Matter. **355**, 188–201 (2005)
27. M.A.L. Nobre, S. Lanfredi, Appl. Phys. Lett. **81**, 451–453 (2002)
28. A.K. Jonscher, *Dielectric relaxation in solids* (Chelsaca Dielectric Press, London, 1983)
29. J. Wang, H. Zhang, D. Xue, Z. Li, J. Phys. D Appl. Phys. **42**, 235103 (2009)
30. A. Shukla, R.N.P. Choudhary, A.K. Thakur, D.K. Pradhan, Phys. B Cond. Matter. **40**, 99–106 (2010)
31. J.T.S. Irvine, D.C. Sinclair, A.R. West, Adv. Mater. **2**, 132–138 (1990)